ARL-TR-8694 • MAY 2019

DEVCOM ARMY RESEARCH LABORATORY

The Ballistic Response of Woven Kevlar Fabric as a Function of Projectile Sharpness

by Julia Cline, Paul Moy, Doug Harris, Jian Yu, and Eric Wetzel

NOTICES

Disclaimers

The findings in this report are not to be construed as an official Department of the Army position unless so designated by other authorized documents.

Citation of manufacturer's or trade names does not constitute an official endorsement or approval of the use thereof.

Destroy this report when it is no longer needed. Do not return it to the originator.

ARL-TR-8694 ● MAY 2019

The Ballistic Response of Woven Kevlar Fabric as a Function of Projectile Sharpness

by Julia Cline, Paul Moy, Doug Harris, Jian Yu, and Eric Wetzel
Weapons and Materials Research Directorate, CCDC Army Research Laboratory

REPORT DOCUMENTATION PAGE

Form Approved
OMB No. 0704-0188

1. REPORT DATE *(DD-MM-YYYY)*	2. REPORT TYPE	3. DATES COVERED (From - To)
May 2019	Technical Report	August 2018

4. TITLE AND SUBTITLE
The Ballistic Response of Woven Kevlar Fabric as a Function of Projectile Sharpness

5a. CONTRACT NUMBER

5b. GRANT NUMBER

5c. PROGRAM ELEMENT NUMBER

6. AUTHOR(S)
Julia Cline, Paul Moy, Doug Harris, Jian Yu, and Eric Wetzel

5d. PROJECT NUMBER

5e. TASK NUMBER

5f. WORK UNIT NUMBER

7. PERFORMING ORGANIZATION NAME(S) AND ADDRESS(ES)
US Army Combat Capabilities Development Command, Army Research Laboratory
ATTN: FCDD-RLW-MB
Aberdeen Proving Ground, MD 21005

8. PERFORMING ORGANIZATION REPORT NUMBER
ARL-TR-8694

9. SPONSORING/MONITORING AGENCY NAME(S) AND ADDRESS(ES)

10. SPONSOR/MONITOR'S ACRONYM(S)

11. SPONSOR/MONITOR'S REPORT NUMBER(S)

12. DISTRIBUTION/AVAILABILITY STATEMENT
Approved for public release; distribution is unlimited.

13. SUPPLEMENTARY NOTES
ORCID ID(s): Julia Cline, 0000-0003-1994-3247; Paul Moy, 0000-0001-5244-6838; Eric Wetzel, 0000-0002-0176-3072; Jian Yu, 0000-0002-1681-4602.

14. ABSTRACT
Right circular cylinders (RCCs) are a common fragment-simulating projectile used to simulate debris resulting from an improvised explosive device (IED) blast. The specifications for ballistic performance of soft body armor specify the geometry and mass of RCC projectiles used for testing. Furthermore, the edges on the impacting side of an RCC projectile have a fillet radius, and recent investigations indicate the fillet radius (or "sharpness") of the projectile may affect the ballistic limit velocity or V_{50}. It is hypothesized that this happens because the sharpness of the projectile changes the fiber-failure mechanism, so to test this, 4-gr RCC projectiles with varying fillet radii (0.635 mm, 1.270 mm, and 1.702 mm) are precisely manufactured. Previously collected, unpublished data for 4-gr RCC projectiles with fillet radii of 0.102 mm, 0.178 mm, and 0.254 mm are also included to assess a range of projectile-sharpness values. Ballistic impact tests on single-layer woven Kevlar K706 fabric are conducted using a laboratory gas gun to measure the V_{50}, which is found to decrease with increasing fillet radii. Impacted specimens are inspected to understand the different failure mechanisms dependent on fillet radius.

15. SUBJECT TERMS
right circular cylinders, RCCs, ballistic limit velocity, Kevlar, projectile sharpness, high-speed camera

16. SECURITY CLASSIFICATION OF:			17. LIMITATION OF ABSTRACT	18. NUMBER OF PAGES	19a. NAME OF RESPONSIBLE PERSON
a. REPORT	b. ABSTRACT	c. THIS PAGE			Julia Cline
Unclassified	Unclassified	Unclassified	UU	43	19b. TELEPHONE NUMBER (Include area code) (410) 306-1949

Contents

List of Figures

List of Tables

Acknowledgments

The authors wish to extend their gratitude to Larry Long (Weapons and Materials Research Directorate [WMRD]) for his help with the experimental setup and specimen preparation; to Parimal Patel (WMRD) and Terrence Taylor (WMRD) for their assistance in gas-gun operation; and to Gary Grimm (US Army Test and Evaluation Command) for lending us the 4-gr gas-gun barrel necessary to complete this work and for his helpful advice.

1. Introduction

Right circular cylinders (RCCs) are a common, nondeformable, fragment-simulating projectile used to simulate debris from blasts of improvised explosive devices (IEDs), land mines, and hand grenades on soft body armor. The Enhanced Combat Helmet (ECH) purchase description[1] outlines the requirements for fragmentation protection (ballistic limit velocity or V_{50}) to a number of projectile threats including several masses of RCCs. The typical geometry of an RCC projectile is specified in the purchase description and shown in Fig. 1. The length (L) and outer diameter (OD) are specified for each weight RCC. For 4-gr (259 mg) RCC projectiles, the specifications are a mass within a tolerance of 0.15 gr (10 mg), OD of 3.40 $\pm$ 0.03 mm, and L of 3.73 mm. The corners of the projectile are filleted as a result of the machining process, with the sharpness of the cutting tool affecting the radius. For 4-gr RCCs, the acceptable fillet radius is 0.178 $\pm$ 0.076 mm.

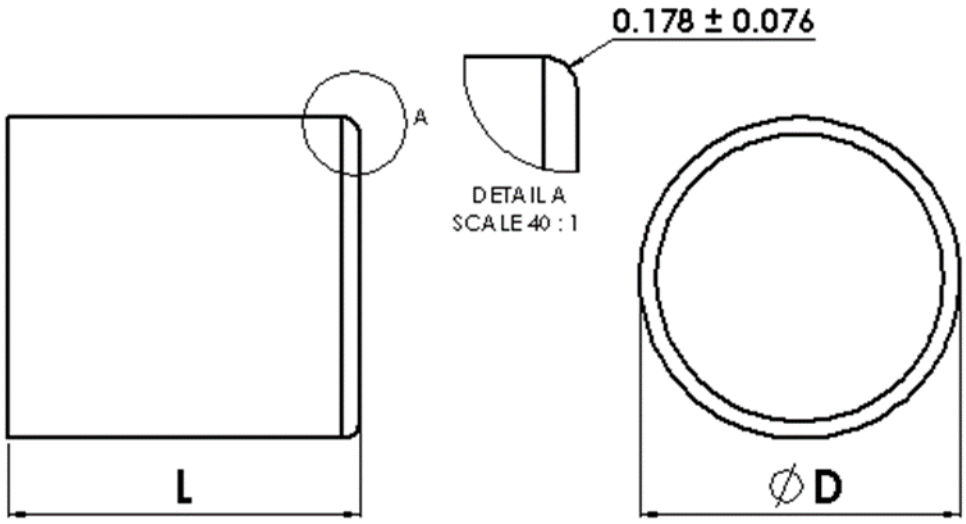

Fig. 1 Geometry of an RCC projectile[1]

A previous, unpublished study of V_{50} for RCC projectiles with precisely machined fillet radii of 4-gr RCC projectiles with fillet radii of 0.102 mm, 0.178 mm, and 0.254 mm indicates the fillet radii may affect the V_{50}, which is the velocity at which 50% of impacting projectiles will penetrate a given target. The cause of this has not been studied extensively and merits further investigation. It is hypothesized that projectile sharpness will govern the mechanism needed to penetrate the fabric, which will affect the V_{50}.

For woven fabrics, such as Kevlar used in soft body-armor protection, there are several mechanisms by which a projectile can penetrate.[2,3] If the yarns are stretched

beyond maximum fiber-failure strain, they will fail in tension. Transverse shear failure of the yarns can occur when a blunt-nosed projectile (e.g., RCC) cuts or shears through the fabric yarns. For loosely woven fabrics or projectiles with smooth curvature (e.g., hemisphere or spherical shape), it is possible for the projectile to push the yarns aside and "window" through the fabric without cutting or failing the yarns.

For computational models aimed at predicting V_0–V_{100} probability curves, realistic failure-mode information is critical to obtaining accurate predictions.[4–8] The goal of this work is to 1) identify if there is a sensitivity to the fillet radii within the current specified tolerance and 2) characterize any systematic trends related to V_{50} and fillet radii in order to better inform fiber/yarn-level computational models of ballistic impact.

2. Approach and Methodology

In this work, we seek to evaluate the effect of projectile sharpness (fillet radii) on the ballistic response of single-layer, scoured-state Kevlar K706 fabric consisting of 60-denier KM2 Kevlar yarns woven at 13 × 13 yarns per cm. Four-grain RCCs with varying fillet radii are machined and accelerated toward the Kevlar targets using a laboratory gas gun to characterize the V_{50}. High-speed digital imaging techniques are used to measure the projectile velocity and yaw angle prior to impact, as well as penetration type on the target's back surface. The impacted targets are examined to discern potential differences in failure mechanisms resulting from the projectile geometry.

2.1 Test Setup

Targets are cut from rolls of Kevlar K706 fabric in 10-cm squares. Care is taken to ensure the fabric is not pulled unevenly during cutting. Targets are mounted on a circular frame and secured using a hose clamp (Fig. 2). A torque wrench is used to secure the bolt at 14 N · m. It is important to ensure the fabric is secured uniformly, not stretched too tightly, and is consistent across all targets tested. A thin black line is drawn on the fabric around the perimeter of the circular frame. Any pull-in of yarns during ballistic impact can be observed as the movement of the lines toward the center of the target.

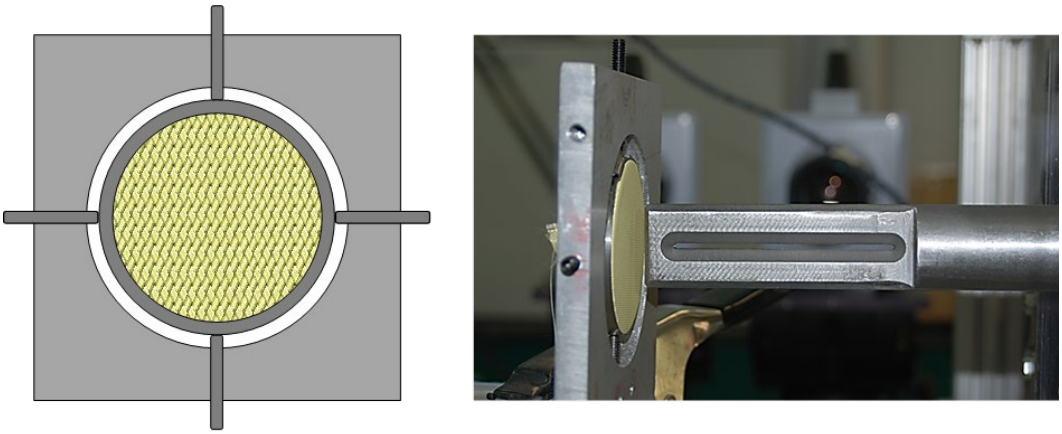

(a) (b)

Fig. 2 a) Target is mounted in a circular mount and secured with set screws before b) being set in place near the barrel of the gas gun.

The circular mount is installed in an aluminum fixture and secured with set screws (Fig. 2a). The fixture is placed on a scissor lift and raised up to align with the center of the barrel (Fig. 2b). A centering tool is used in conjunction with a laser shone down the barrel to fine-tune the alignment to ensure the projectile will impact on dead center of the target. The fixture is secured to the scissor lift using clamps to ensure it does not move during testing.

A full schematic of the experimental setup is shown in Fig. 3. A 4-gr, 3.40-mm diameter barrel is installed on a laboratory gas gun with the end of the barrel set at 7.1 mm from the target. A 10-cm slot (Fig. 2b) at the end of the barrel allows for high-speed imaging of the projectile before it leaves the barrel and impacts the target. A block of ballistic gel (Perma-Gel) is set behind the target to catch projectiles that completely penetrate the target.

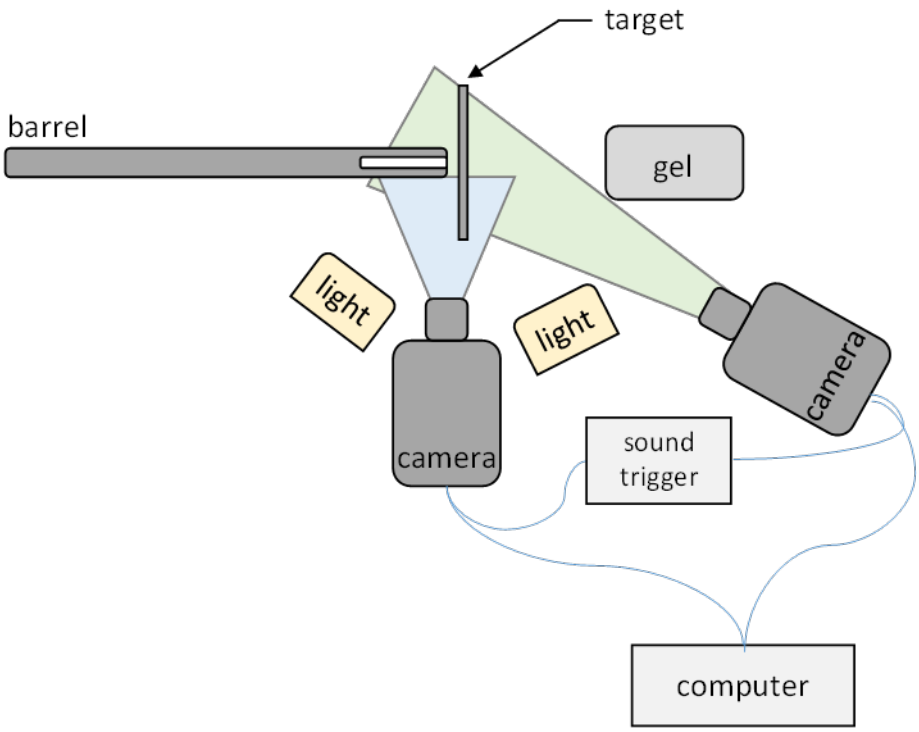

Fig. 3 Experimental setup for V_{50} testing

A Photron Fastcam SA5 high-speed camera is set up perpendicular to the end of the barrel such that the imaged area focuses on a portion of the slot opening and the spacing between the barrel and target (Fig. 4a). The frame rates used for image capture are summarized in Table 1. The frame rate and exposure time are adjusted based on the impact velocities to ensure capture of focused images with minimal blur of the projectile moving through the barrel.

A second high-speed camera (Photron Fastcam SA1) is set up behind the target, angled such that it can capture the back surface of the target. Setting the camera at an off angle ensures the camera is not in the direct path of projectiles. A frame rate of 72,000 fps is used. A sample image showing a complete penetration of a hemispherical 1.702-mm fillet radii projectile is shown in Fig. 4b.

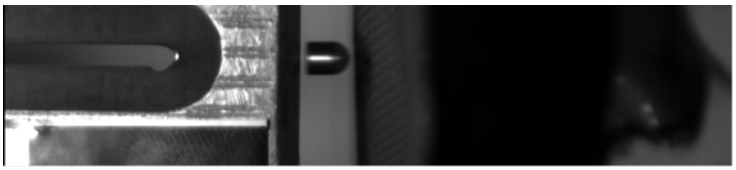

(a)

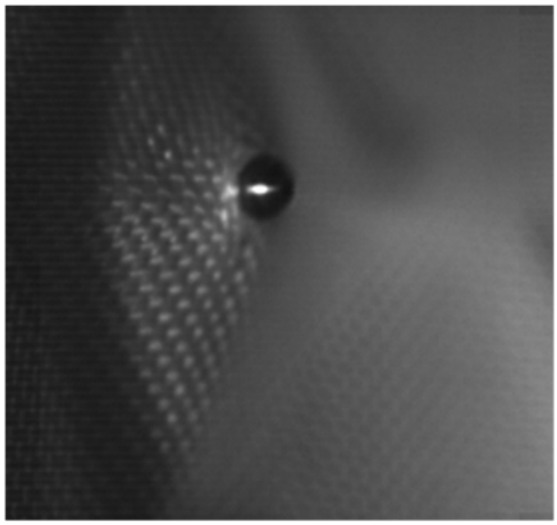

(b)

Fig. 4 Example images of the view from the a) side camera and b) back-surface camera

Table 1 Frame rate and exposure-time settings for Photron Fastcam SA5 to measure projectile impact velocity

Frame rate (fps)	Exposure time (μs)	Projectiles
93,000	10.51	1.702-mm RCCs
150,000	6.42	0.635-mm, 1.270-mm RCCs
210,000	3.96	0.635-mm RCCs

Two continuous high-intensity LED light (Veritas, Inc) sources are used to provide sufficient lighting for the cameras during testing. A sound trigger (Kapture Group) set at the highest gain sensitivity is used to trigger both cameras when the gas gun expels from the pressure tank into the barrel.

2.2 Projectiles

The RCC projectiles are precisely machined by Best Machine Co, Inc (Edgewood, Maryland) with fillet radii of progressively decreasing sharpness as shown in Fig. 5. The sharpest projectiles seek to evaluate the lower and upper bounds of the RCC specifications to see if there are differences in V_{50} and failure mechanisms within the specified tolerance. These were tested previously and the results are included here for comparison with tests conducted in this study. The geometry of the projectiles is superimposed on an image of K706 woven fabric for comparison of the fillet with yarn size in Fig. 6. To maintain the mass of each RCC, the length varies slightly among projectiles.

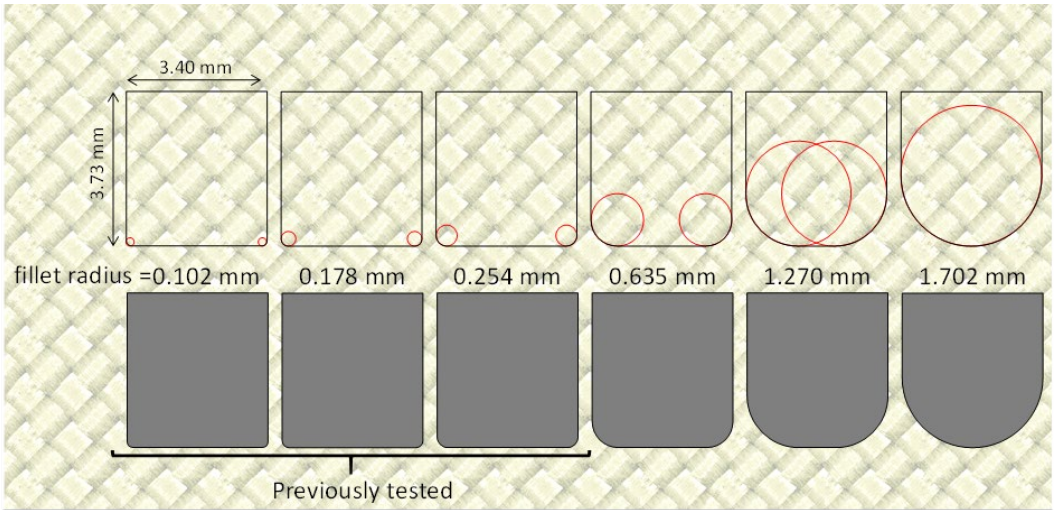

Fig. 5 Geometry of the RCC projectiles with varying fillet radii manufactured for this study

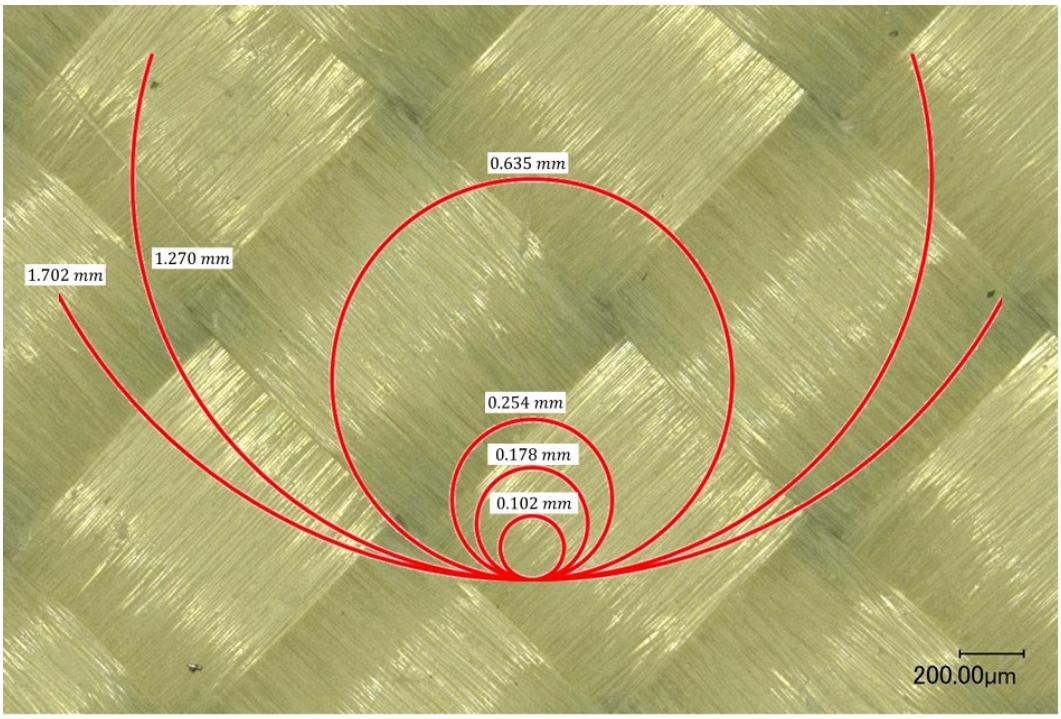

Fig. 6 Comparison of the fillet radii with the size of the yarns in a Kevlar woven fabric

The mass of a sample (30 RCCs) of each RCC variety is measured using a Mettler Toledo Scale AT201 (capacity 205 g, d-0.02 mg). All RCCs are within the tolerance specified (4 ± 0.15 gr); however, a larger variation in the mass is measured for the hemispherical, 1.702-mm fillet radii RCCs (Fig. 7). Therefore, each hemispherical RCC projectile is weighed before testing and any outside the tolerance are discarded. All projectiles are manufactured from AISAI 4340 heat-treated to Rockwell "C" hardness of 29 ± 2. The slight variation in mass among the projectiles does not cause a discernable increase in impact energy.

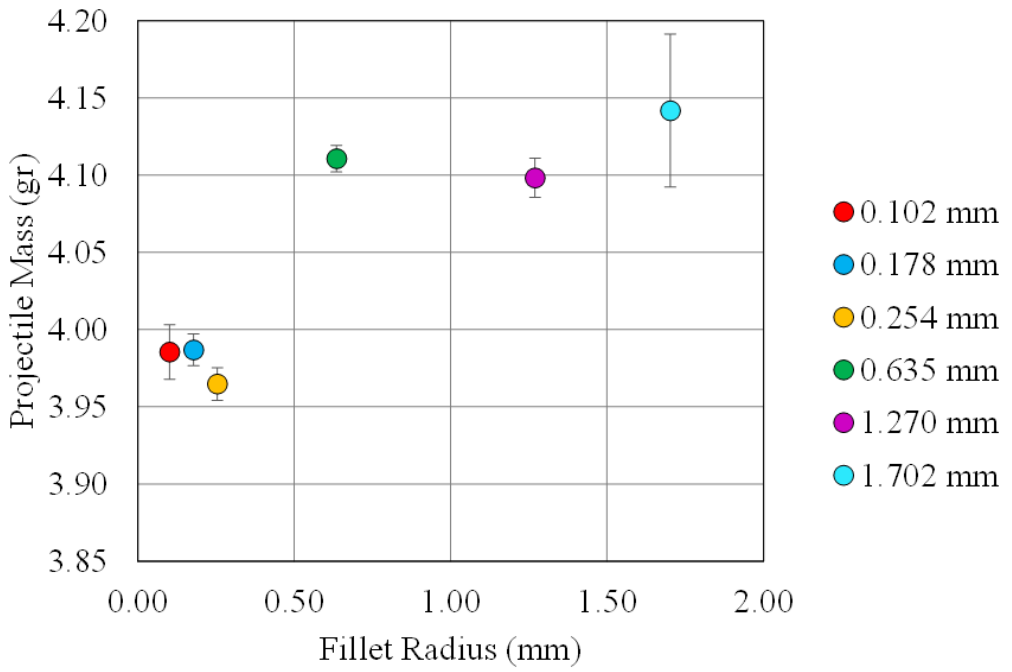

Fig. 7 Variation in mass of RCC projectiles measured prior to testing

The fillet radii are measured for a sample of projectiles (10 RCCs) using a Keyence VHX-2000 optical microscope to assess the consistency and symmetry. Two measurements were obtained from each corner of profile images of the RCC (see Fig. 8). It appears the average radii tend to be about 0.025 mm more for the standard RCC. Here the assumption is that during the machining of the smaller-radii RCCs, it is more likely to have more material removed by the tooling bit than it is to remain at the minor tolerance value. Whereas the 0.635-, 1.270-, and 1.702-mm RCCs appear to have a much narrower tolerance (see Table 2).

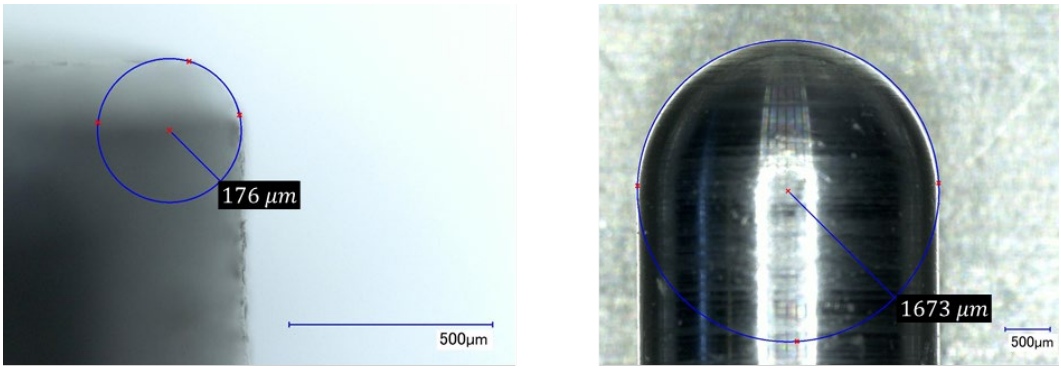

(a) (b)

Fig. 8 Fillet radius measurements for a) 0.102-mm RCC and b) 1.702-mm RCC

Table 2 Measurements of fillet radii for RCC projectiles via optical microscopy

Desired RCC fillet radii (mm)	Average measured fillet radii (mm)	Standard deviation	COV (%)
0.102	0.132	0.010	7.72
0.178	0.218	0.015	6.96
0.254	0.297	0.018	5.99
0.635	0.617	0.028	4.52
1.270	1.328	0.020	1.53
1.702	1.671	0.005	0.31

2.3 Velocity Measurement

The distance measurement tool in the Photron Fastcam software is used to extract displacement measurements, which are used to calculate the projectile velocity. The tool must first be calibrated by selecting two points that are a known distance apart in the picture. In our work, a piece of tape stuck to the end of the barrel measuring exactly 2.54 cm long is used to calibrate the distance-measurement tool. The distance the front of the projectile travels ($\Delta d = d_2 - d_1$) between a certain number of frames, n, is measured and the velocity, v, is calculated from Eq. 1, where fps is the frame rate.

$$v = \frac{\Delta d}{n} \times \text{fps} \tag{1}$$

SenTest[9] software is used to guide target velocity choices. SenTest is based on the Neyer D-Optimal test method and is a generic software designed for conducting and analyzing sensitivity tests. In our work, we specify the initial guesses for the bounds of the velocity measurements and the SenTest software selects target velocity values to test based on whether the previous velocity test was a success (complete penetration) or failure (partial penetration). The software is fairly independent of the initial guess; however, for efficiency of testing, it is recommended the initial guess values are close to the target values. The initial guesses used in our work are $\mu_{min} = 50\ m/s$; $\mu_{max} = 200\ m/s$; and $\sigma_{guess} = 10\ m/s$, where μ is the quantity of interest, V_{50}, and σ is the standard deviation.

2.4 Experimental Considerations

Achieving a tight seal around the projectiles such that all of the force from the expanding helium gas is used to accelerate the projectiles toward the target proves more difficult than expected for RCCs with the 0.635-mm and 1.270-mm fillet

radii. As seen in Fig. 9, a relatively linear velocity–pressure curve is achieved for the hemispherical, 1.702-mm RCC projectiles, which makes it easy to predict the pressure needed to achieve a target velocity. This is not the case for the 0.635-mm RCC projectiles. It is thought the 0.635-mm RCC projectiles may be slightly undersized for the barrel, allowing helium to escape around the projectile and effectively reducing the pressure. The release of gas ahead of the projectile can be seen in the high-speed camera images as the piece of tape will flutter from the expelled gas. The use of a cork plug inserted behind the projectile improves the seal around the projectile and allows for more consistent velocity–pressure data. The cork plugs were punched from a 6.35-mm-thick sheet and were slightly larger than the barrel diameter so that they fit snugly. A new cork plug is used for each shot. The cork plug decelerates faster than the projectile in the barrel and thus does not add any parasitic weight to the projectile during impact.

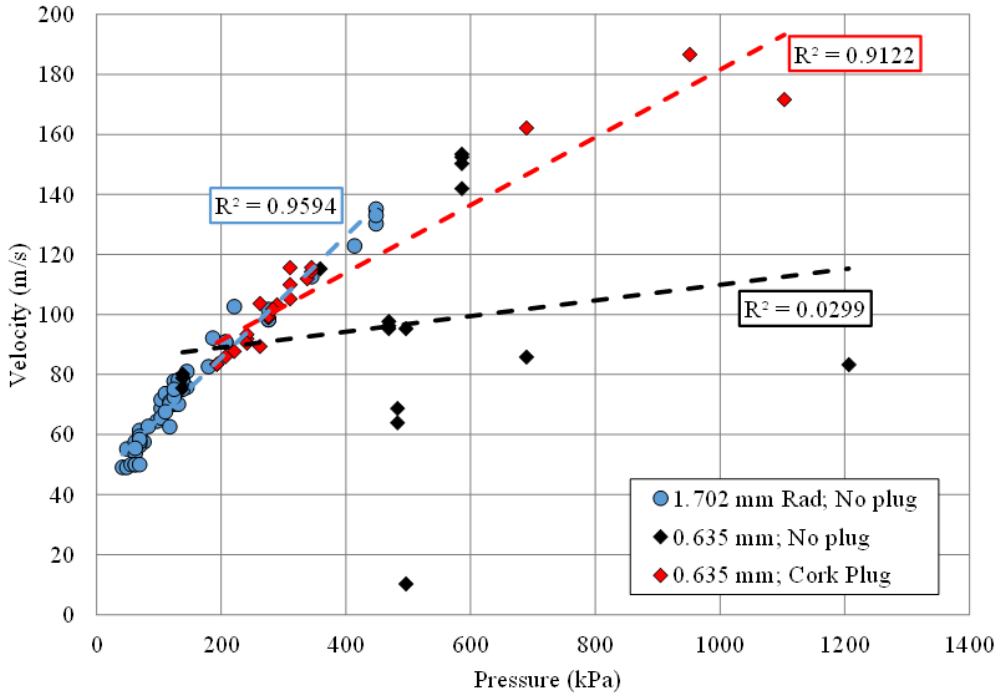

Fig. 9 Velocity–pressure measurements

3. Results and Discussion

Approximately 40 shots per projectile geometry are taken and any shots with significant yaw prior to impact are disregarded in the V_{50} calculation. Full data tables of velocity categorized with penetration type are found in the Appendix. Figure 10 shows the velocity data plotted versus penetration type (1, complete; 0, partial) for all RCC projectiles. The V_{50} and standard deviation are calculated using

the SenTest software and shown visually in Fig. 10 with a dashed red line. The zone of mixed results is defined as the region between the lowest complete-penetration and highest partial-penetration velocities. This zone is narrowest for the 1.270-mm and 1.702-mm fillet radius RCCs and widest for the 0.635-mm and 0.254-mm fillet radius RCCs.

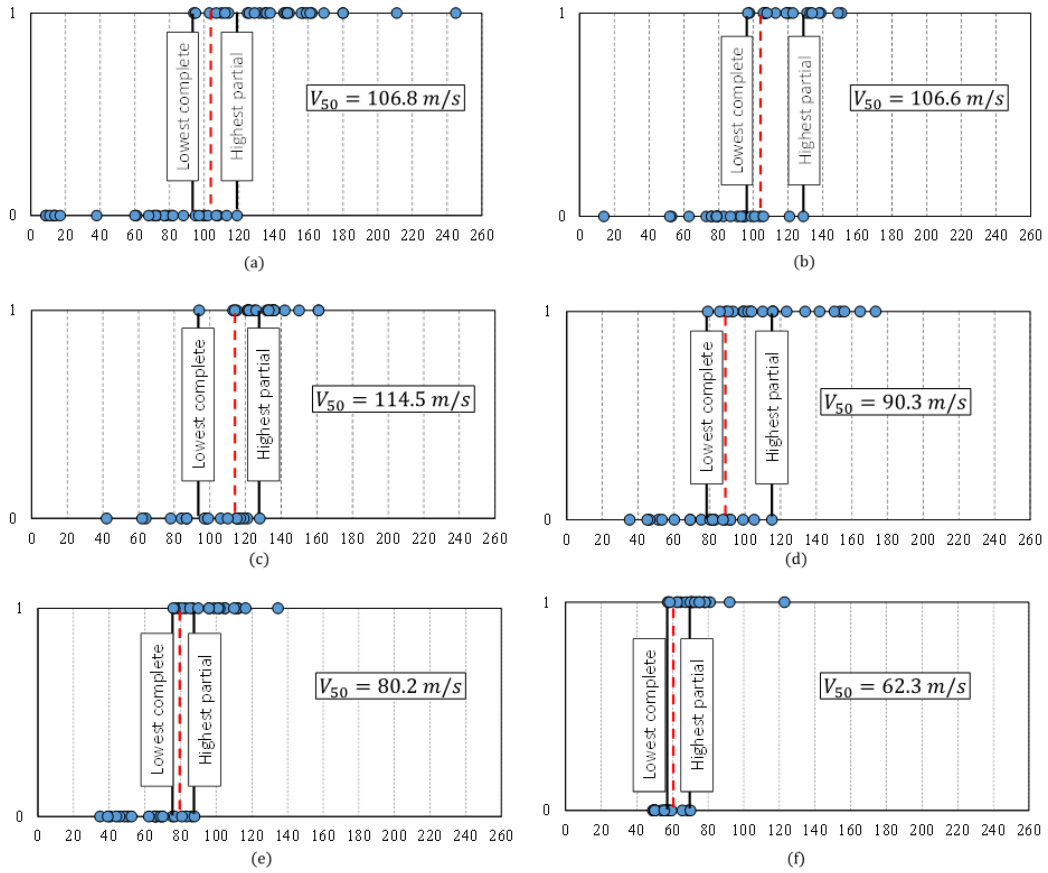

Fig. 10 Velocity and penetration type for RCCs with fillet radius of a) 0.102 mm, b) 0.178 mm, c) 0.254 mm, d) 0.635 mm, e) 1.270 mm, and f) 1.702 mm

Figure 11 plots the V_{50} as a function of fillet radius and a clear linear relationship can be identified. The V_{50} decreases with increasing fillet radius or, alternatively, the V_{50} increases with projectile sharpness.

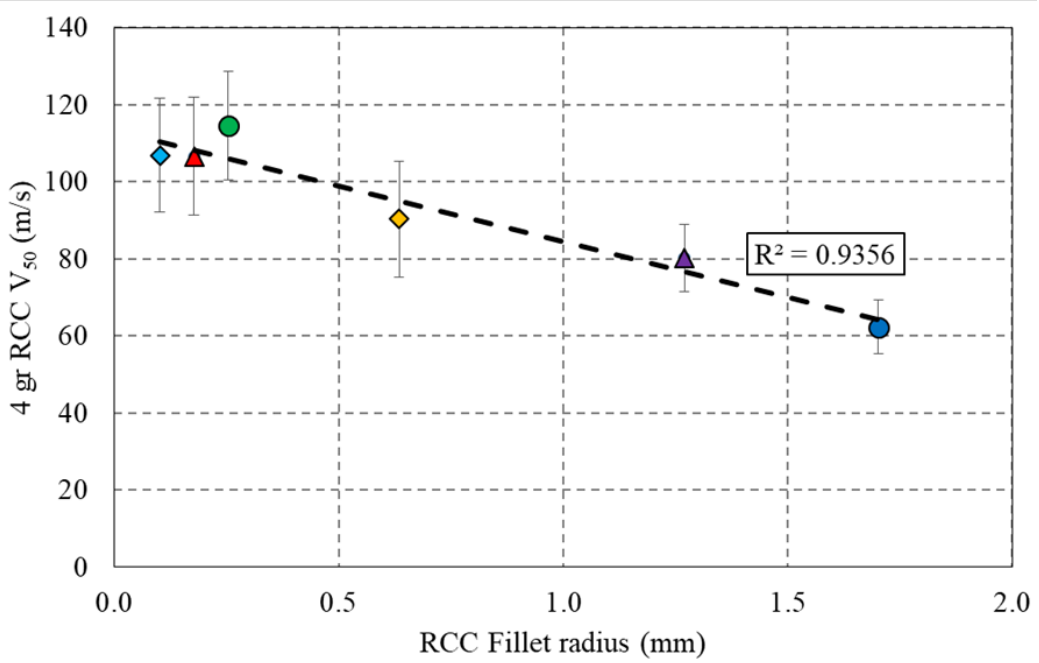

Fig. 11 Measured V_{50} for each fillet radius

Figure 12 shows the probability of complete penetration as a function of impact speed. The error bars denote one standard deviation from the mean value. There is overlap in the error bars but there is a clear difference in the limit velocities for each fillet radii (except the 0.102 mm and 0.178 mm). The V_{50} values for the sharpest projectiles (0.102 mm, 0.178 mm, and 0.254 mm) are all within the error of each other.

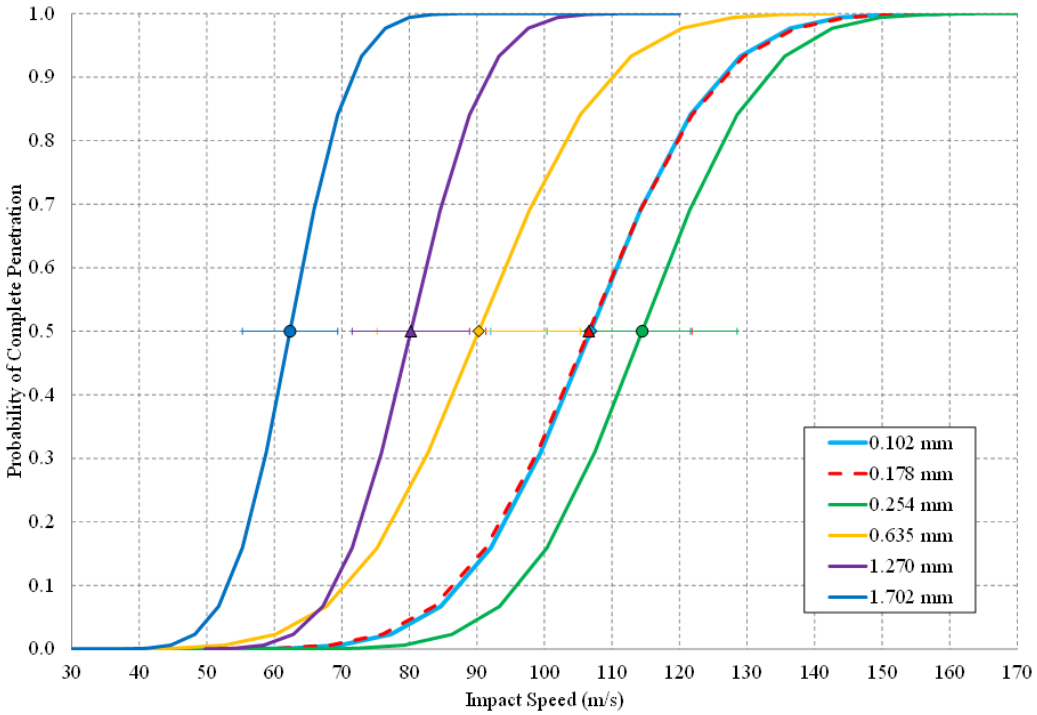

Fig. 12 Probability of penetration as a function of impact speed for all projectiles tested

The probability of penetration of a dull, rounded projectile is high at low velocities. This is because the smoother, hemispherical projectiles can more easily poke through the gaps in the weave and spread a yarn open without breaking fibers. The location on the weave at which the projectile impacts on the fabric makes a difference in the damage visible on the tested specimen. Figure 13 shows the back-camera images of two partially penetrating shots at the same velocity (50 m/s). Fig. 13a shows the impact location is between two vertical yarns and impacts directly on the horizontal principal yarn, whereas the impact in Fig. 13b appears to be at the cross of two yarns. Figures 13c and d show the back side's damage area for each impact. Despite having the same impacting kinetic energy, the damage differs significantly based on the impact location.

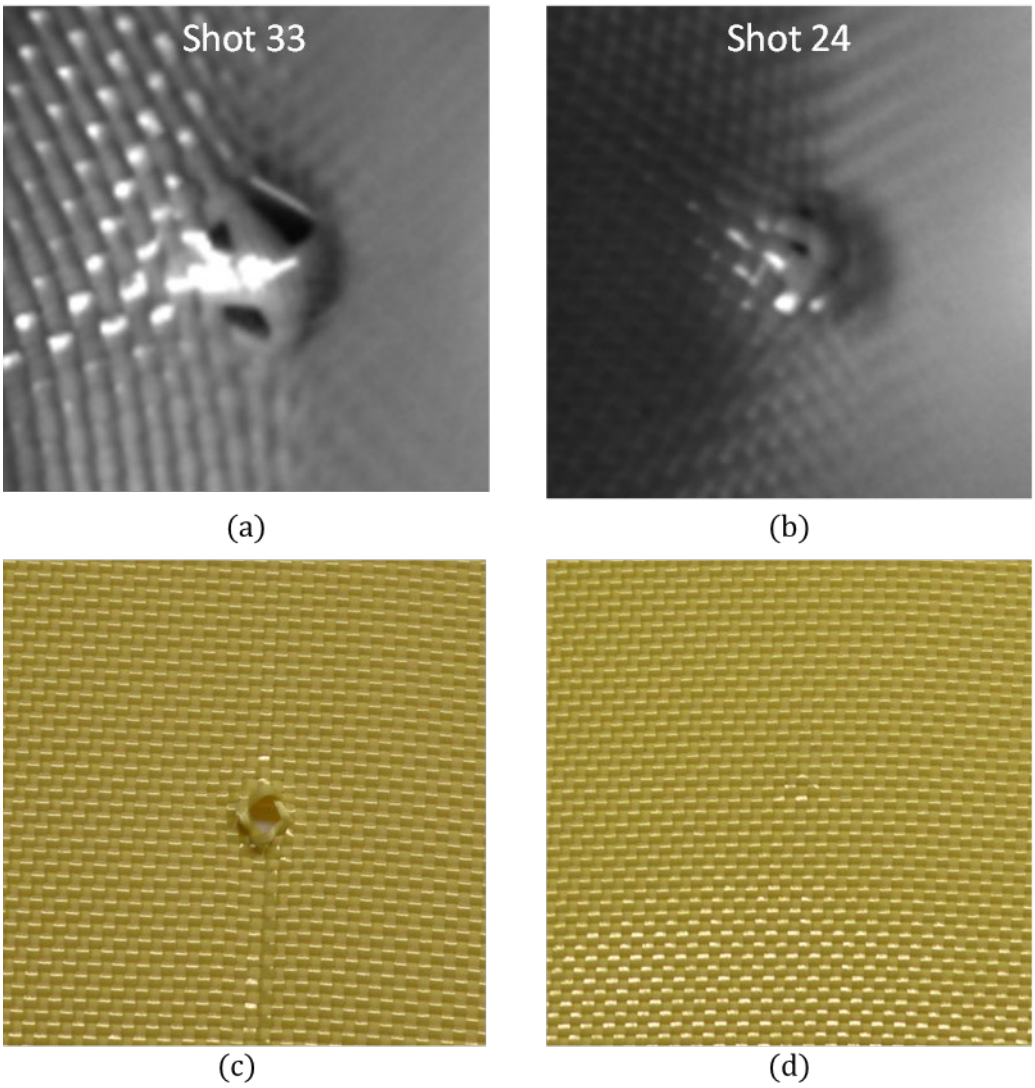

Fig. 13 Images a) and b) are 1.702-mm fillet radius RCCs partially penetrating targets and c) and d) are their corresponding targets after impact

As velocities increase to the V_{50} and above, the projectiles seem to more easily penetrate through the fabric either by windowing through a gap in the weave (Fig. 14a) or by the yarn sliding around the projectile (Fig. 14b). For higher velocity shots (Fig. 15a), the projectile's kinetic energy is enough to significantly pull the principal yarns from the frame (Fig. 15b), causing significant damage on the back surface (Fig. 15c) but without any evidence of broken fibers due to tensile failure.

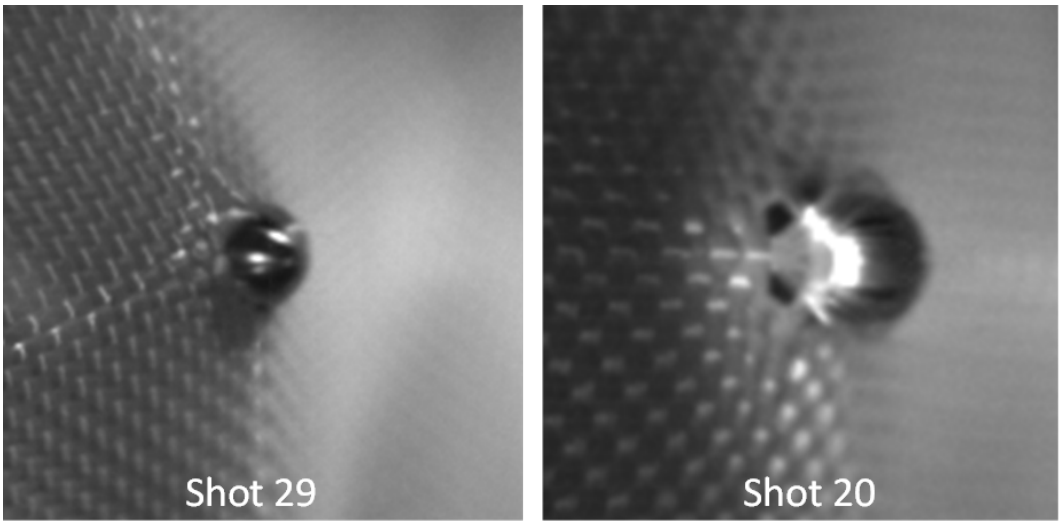

Fig. 14 Hemispherical nose projectiles can defeat the target by a) windowing through the fabric or b) yarns sliding around the projectile

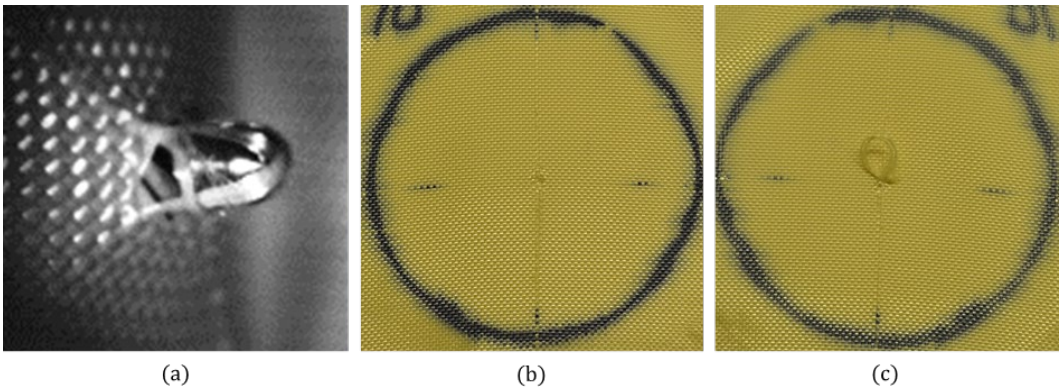

Fig. 15 Back-surface image of 1.702-mm fillet-radius RCC projectile (Shot 10) shows a) projectile pulling primary yarns as it penetrates the fabric, which can be observed on the b) front and c) back surface of the target after impact

As the fillet radius becomes sharper, more principal yarns are engaged in the impact event. Figure 16 shows two impacts with a 1.270-mm fillet-radius RCC projectile. The partial penetrating shot shown in Fig. 16a engages two principal yarns in the horizontal and vertical directions. Some sliding of the yarns around the projectile still occurs, as can be seen in Fig. 16b. Back-surface damage for each of these shots is shown in Figs. 16c and d. However, in both of these cases there is no significant evidence of yarn failure. For higher-velocity completely penetrating shots, a few broken fibers can be seen on the back surface of the fabric but complete yarn failure is not occurring.

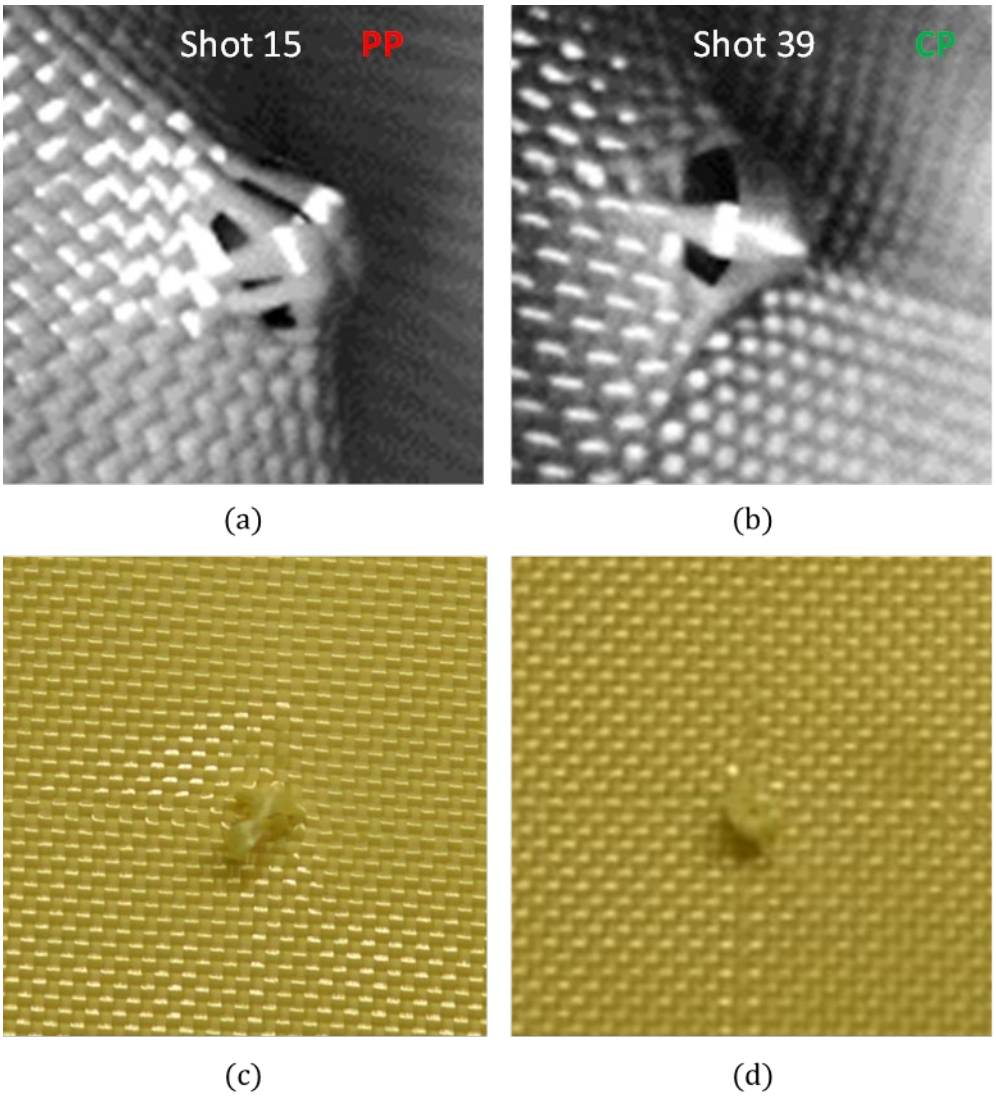

Fig. 16 Back-surface images and impacted targets for 1.270-mm fillet-radius RCC projectile shot near V_{50}: a) and c) are partial penetration and b) and d) are complete penetration

The trend continues for the 0.635-mm fillet radius RCCs as Fig. 17 illustrates. This is a complete-penetration impact event involving multiple principal yarns. Significant pull-out of the fiber from the frame is evident by the large loops of yarn on the back surface of the fabric. For higher-velocity completely penetrating shots, we start to see some broken yarns on the back surface of the fabric as shown in Fig. 18. For partial impacts, we start to notice more permanent deformation on the front and back surfaces of the fabric targets indicative of the blunt nose of the RCC projectile (Fig. 19).

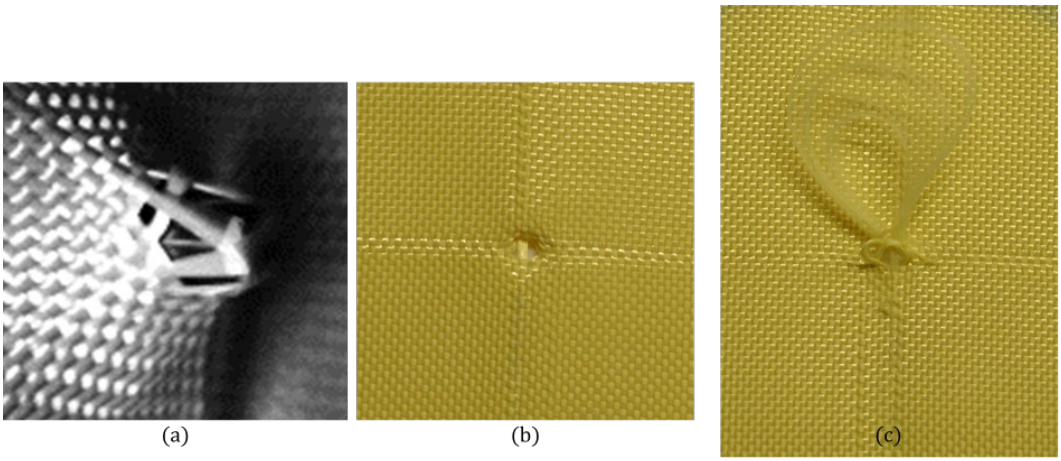

Fig. 17 Back-surface and impacted-target images for a 0.635-mm fillet-radius RCC projectile (Shot 30) that completely penetrated the target at 102 m/s

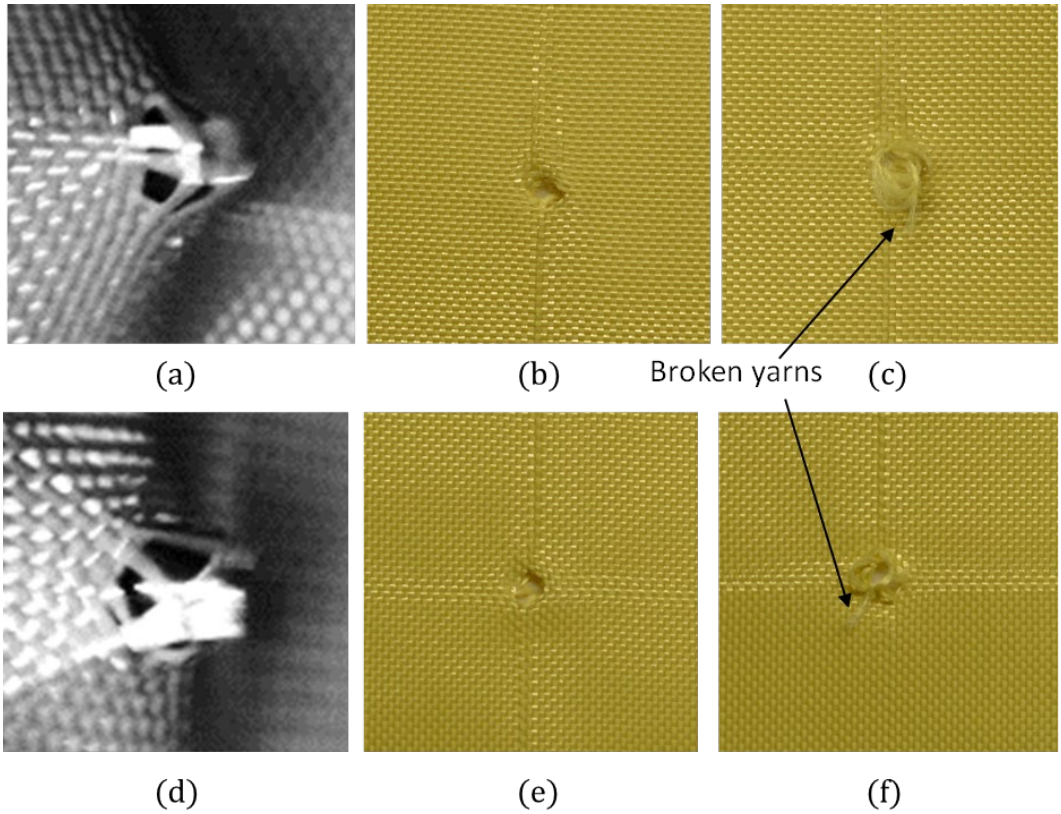

Fig. 18 Completely penetrating 0.635-mm fillet-radius RCCs show damage and broken yarns: a) back surface and impacted target b) front and c) back for Shot 20 (v = 116 m/s), and d) back surface and impacted target e) front and f) back for Shot 12 (v = 165 m/s)

Fig. 19 Partially penetrating impact by a 0.635-mm fillet-radius RCC travelling at 105 m/s (Shot 22) viewed from the back surface a); impacted target shows permanent deformation on the b) front and c) back surfaces

Images of the back surface of the fabric during impact are not available for the RCCs with fillet radii of 0.102 mm, 0.178 mm, and 0.254 mm; so, we are unable to ascertain where the projectile impacts the fabric. However, post mortem images of the impacted targets help in understanding what is occurring during an impact event.

Figure 20 shows the back surface of two fabrics impacted at the same velocity, both penetrating shots. Multiple principal yarns are engaged and there is some pull-in of the yarns from the frame. Figure 21 shows the front and back surface-damage areas of two shots at 115 m/s, which is approximately the measured V_{50} for the 0.2540-mm projectile. Figure 21a is a partial penetration; Figure 21c is a complete penetration. The damage on the back surface differs depending on the penetration type.

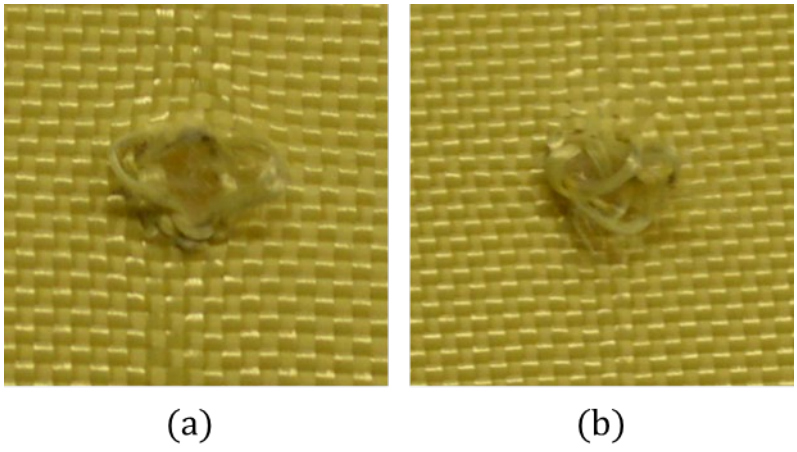

Fig. 20 Back surfaces of impacted targets of two completely penetrating shots at 136 m/s: a) Shot 39 and b) Shot 31 for RCCs with a 0.254-mm fillet radius

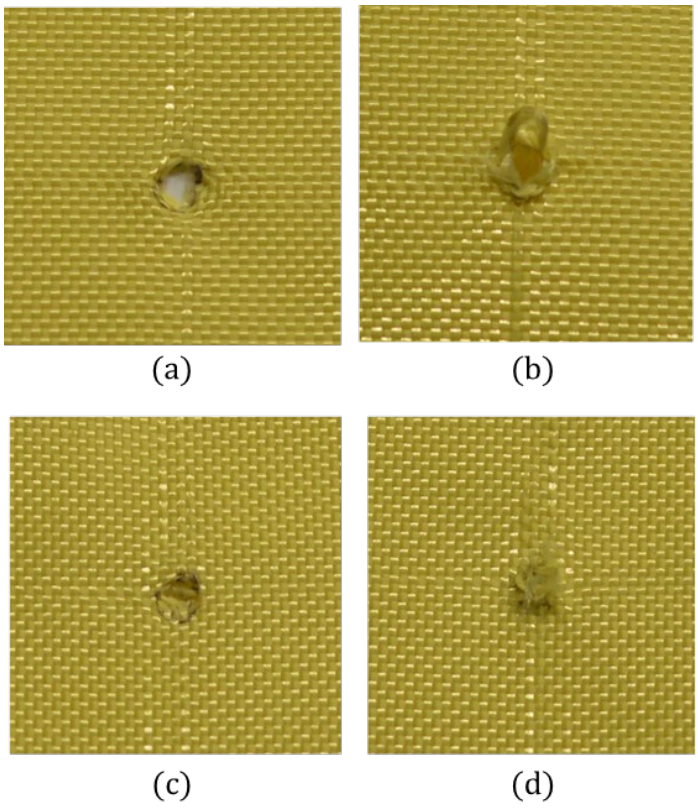

Fig. 21 Images a) and c) front and b) and d) back of targets impacted at 115 m/s with a 0.254-mm fillet radius RCC; a) and b) are partially penetrating Shot 10, c) and d) are completely penetrating Shot 29

For the sharpest projectiles, evidence of broken yarns during completely penetrating shots is more apparent. Figure 22a and b show the back surfaces of sample fabric targets for 0.178-mm and 0.102-mm fillet radius RCC projectiles, respectively.

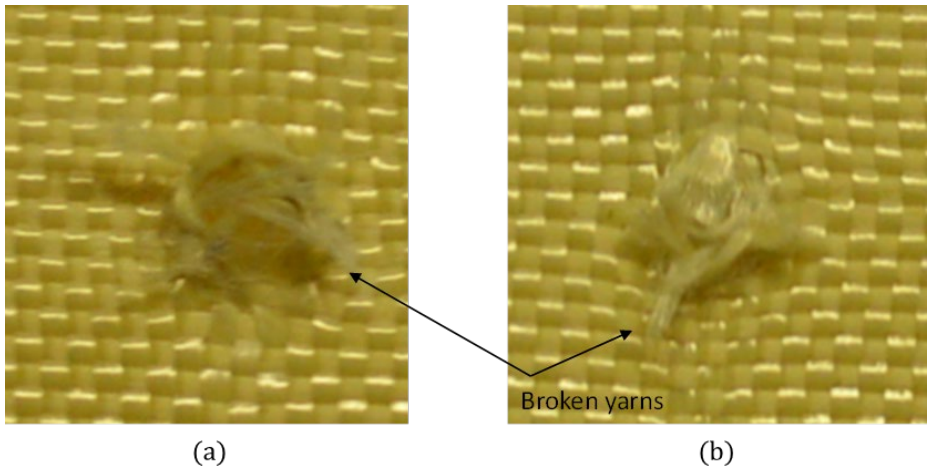

Fig. 22 Back-surface images of completely penetrated targets show broken yarns after impact with a) 0.178-mm (Shot 2) and b) 0.102-mm (Shot 1) RCC projectiles

The data show a transition with increasing projectile sharpness from a windowing-failure mode to yarn failure via transverse shearing. This agrees with the trend of V_{50} increasing with increasing projectile sharpness. As the projectile becomes sharper (or more blunt nosed) it cannot slip through or window through the fabric, so it must expend more energy to break the yarns to penetrate the material, thus increasing the ballistic performance of the fabric for that threat.

4. Conclusions

In this work, we evaluate the effect of projectile sharpness on the V_{50} for single-layer, scoured-state Kevlar K706 fabric consisting of 60-denier KM2 Kevlar woven at 13 × 13 yarns per cm. RCC projectiles of fillet radii ranging from sharp (0.102 mm) to dull (1.702 mm–hemispherical) are precisely manufactured and the geometry is verified using a Keyence microscope. A laboratory helium-gas gun accelerates projectiles toward the fabric targets and high-speed digital cameras capture the projectile as it exits the barrel and impacts on the fabric as well as the back surface of the fabric during impact. Analysis of the images of the projectile allows for the calculation of the projectile velocity and determination of the yaw angle. Projectiles that yaw before impact are regarded as bad shots and their velocities are not included in the V_{50} calculation. Limit velocities for each projectile geometry are calculated using SenTest.

The V_{50} increases linearly with increasing projectile sharpness. This is likely because the smoother, duller projectiles (1.702-mm radius) can more easily penetrate the woven Kevlar fabric by windowing through gaps in the weave or by yarns slipping over the projectile nose. The back-surface images confirm the yarns spread apart around the projectile as it penetrates. Higher-velocity projectiles also significantly pull principal yarns from the frame, causing significant damage to the fabric but without breaking fibers. To elicit tensile failure in the fibers, we could try to more tightly clamp the fabric into the frame; however, the likelihood of yarn failure at the boundary would increase.

As projectile sharpness increases, more yarns are engaged in defeating the projectile during the impact event due to the increasingly blunt shape of the impact area. For the sharpest projectiles, we see yarn breakage due to transverse shearing for high-velocity complete penetrations. For blunt-nosed projectiles, it is unlikely they will window through the fabric or that the yarns will slip over the surface. This is an explanation for the trend we see in V_{50} values. More energy must be expended to penetrate the material for sharper fillet-radii projectiles, which increases the ballistic protection performance of the fabric to that specific threat.

There is a systematic transition in failure mechanism observed from yarn pull-out and windowing failure to transverse shearing of yarns as projectile sharpness increases.

It was hypothesized that we would observe tensile failure of the yarns for the hemispherical-projectile impacts; however, we were unable to introduce tensile failure of the yarns due to the significant pull-out of the yarns from the frame during impact and the ease at which the projectile could window through the fabric. Potential future work could include repeating tests with epoxy-impregnated Kevlar fabric or ultra-high molecular weight polyethylene (UHMWPE) cross-ply material to suppress the projectiles' ability to window through the fabric. The characterization of the effect of projectile sharpness on the V_{50} for gel-spun, fiber-based UHMWPE cross-ply or solid-state extruded-polyethylene materials would be of interest as they represent the state-of-the-art materials used in Soldier body armor and head protection today.

5. References

1. Department of the Army. Purchase description enhanced combat helmet (ECH), PD-ECH-ICE-PG16-0001. Quantico (VA): Project Manager–Infantry Combat Equipment, Department of the Army (US); 2009.

2. Nilakantan G, Merrill R, Keefe M, Gillespie J, Wetzel E. Experimental investigation of the role of frictional yarn pull-out and windowing on the probabilistic impact response of Kevlar fabrics. Comp Part B: Eng. 2015;68:215–229.

3. Nilakantan G, Wetzel E, Bogetti T, Gillespie J. A deterministic finite element analysis of the effects of projectile characteristics on the impact response of fully clamped flexible woven fabrics. Comp Struc. 2013;95:191–201.

4. Nilakantan G. Experimentally validated predictive finite element modelling of the V0-V100 probabilistic penetration response of a Kevlar fabric against a spherical projectile. Int J Prot Struc. 2018;9(4):504–524.

5. Nilakantan G, Horner S, Halls V, Zheng J. Virtual ballistic impact testing of Kevlar soft armor: predictive and validated finite element modeling of the V0-V100 probabilistic penetration response. Def Tech. 2018;14(3):213–225.

6. Duan Y, Keefe M, Bogetti T, Powers B. Finite element modeling of transverse impact on a ballistic fabric. Int J Mech Sci. 2006;48(1):33–43.

7. Rao M, Duan Y, Keefe M, Powers B, Bogetti T. Modeling the effects of yarn material properties and friction on the ballistic impact of a plain-weave fabric. Comp Struc. 2009;89(4):556–566.

8. Sun D, Chen X, Lewis E, Wells G. Finite element simulation of projectile perforation through a ballistic fabric. Tex Res J. 2012;83(14):1489–1499.

9. MIL-STD-662F. Test method standard: V_{50} ballistic test for armor. Washington (DC): Department of Defense (US); 1997 Dec 18.

Appendix. Full Data Tables of Velocity Categorized with Penetration Type

Table A-1 Velocity and penetration type for 4-gr RCC 0.1016-mm fillet radius projectiles

Shot no.	Velocity (m/s)	Penetration
1	245	complete
2	211	complete
3	8.8	partial
4	146	complete
5	8.8	partial
6	180	complete
7	61	partial
8	13	partial
9	125	complete
10	110	complete
11	14	partial
12	126	complete
13	94	complete
14	11	partial
15	88	partial
16	119	partial
17	103	complete
18	95	partial
19	14	partial
20	162	complete
21	17	partial
22	100	partial
23	157	complete
24	95	complete
25	78	partial
26	38	partial
27	100	partial
28	169	complete

Table A-1 Velocity and penetration type for 4-gr RCC 0.1016-mm fillet radius projectiles (continued)

Shot no.	Velocity (m/s)	Penetration
29	60	partial
30	73	partial
31	81	partial
32	77	partial
33	156	complete
34	132	complete
35	135	complete
36	159	complete
37	161	complete
38	136	complete
39	82	partial
40	138	complete
41	149	complete
42	107	complete
43	180	complete
44	108	partial
45	114	complete
46	129	complete
47	102	partial
48	112	complete
49	147	complete
50	148	partial
51	71	partial
52	72	partial
53	68	partial
54	97	partial

Table A-2 Velocity and penetration type for 4-gr RCC 0.1778-mm fillet radius projectiles

Shot no.	Velocity (m/s)	Penetration
1	14	partial
2	151	complete
3	149	complete
4	73	partial
5	91	partial
6	95	partial
7	129	partial
8	107	complete
9	80	partial
10	104	partial
11	131	complete
12	76	partial
13	121	complete
14	83	partial
15	120	complete
16	53	partial
17	139	complete
18	76	partial
19	107	complete
20	133	complete
21	63	partial
22	52	partial
23	79	partial
24	138	complete
25	95	partial
26	79	partial
27	95	partial

Table A-2 Velocity and penetration type for 4-gr RCC 0.1778-mm fillet radius projectiles (continued)

Shot no.	Velocity (m/s)	Penetration
28	121	partial
29	93	partial
30	99	partial
31	119	complete
32	134	complete
33	113	complete
34	101	partial
35	98	complete
36	87	partial
37	79	partial
38	97	complete
39	107	complete
40	123	complete
41	106	complete
42	108	complete
43	106	partial

Table A-3 Velocity and penetration type for 4-gr RCC 0.2540-mm fillet radius projectiles

Shot no.	Velocity (m/s)	Penetration
1	150	complete
2	136	complete
3	121	partial
4	116	partial
5	135	complete
6	78	partial
7	135	complete

Table A-3 Velocity and penetration type for 4-gr RCC 0.2540-mm fillet radius projectiles (continued)

Shot no.	Velocity (m/s)	Penetration
8	125	complete
9	64	partial
10	115	partial
11	161	complete
12	121	complete
13	84	partial
14	119	partial
15	142	complete
16	132	complete
18	133	complete
19	98	partial
20	113	complete
22	161	complete
23	106	partial
24	121	complete
25	87	partial
26	122	complete
27	97	partial
28	94	complete
29	115	complete
30	99	partial
31	136	complete
32	117	partial
33	115	partial
34	128	partial
35	122	complete
36	110	partial

Table A-3 Velocity and penetration type for 4-gr RCC 0.2540-mm fillet radius projectiles (continued)

Shot no.	Velocity (m/s)	Penetration
37	122	complete
38	62	partial
39	136	complete
40	133	complete
41	126	complete
42	87	partial
43	42	partial
44	114	complete

Table A-4 Velocity and penetration type for 4-gr RCC 0.6350-mm fillet radius projectiles

Shot no.	Velocity (m/s)	Penetration
1	92	partial
2	83	partial
3	51	partial
4	60	partial
6	53	partial
7	156	complete
8	173	complete
9	123	complete
10	35	partial
11	45	partial
12	165	complete
13	69	partial
14	134	complete
15	79	complete
16	89	partial

Table A-4 Velocity and penetration type for 4-gr RCC 0.6350-mm fillet radius projectiles (continued)

Shot no.	Velocity (m/s)	Penetration
17	81	partial
18	82	partial
19	69	partial
20	116	complete
21	116	complete
22	105	partial
23	110	complete
24	116	complete
25	99	complete
26	99	partial
27	99	complete
28	103	complete
30	102	complete
31	89	complete
32	104	complete
33	92	partial
34	93	complete
35	90	complete
36	88	partial
37	86	complete
38	42	partial
39	83	partial
40	83	complete

Table A-5 Velocity and penetration type for 4-gr RCC 1.270-mm fillet radius projectiles

Shot no.	Velocity (m/s)	Penetration
1	96	complete
2	99	complete
3	70	partial
4	66	partial
5	83	complete
6	79	complete
7	50	partial
8	48	partial
9	87	complete
10	86	partial
11	66	partial
12	83	partial
13	81	complete
14	75	partial
15	77	complete
16	40	partial
17	53	partial
18	35	partial
19	77	partial
20	65	partial
21	112	complete
22	112	complete
23	85	complete
24	135	complete
25	62	partial (capture)
26	116	complete
27	105	complete

Table A-5 Velocity and penetration type for 4-gr RCC 1.270-mm fillet radius projectiles (continued)

Shot no.	Velocity (m/s)	Penetration
28	105	complete
29	76	complete
30	46	partial
31	110	complete
32	88	partial
33	69	partial
34	44	partial
35	39	partial
37	90	complete
38	102	complete
39	101	complete
40	96	complete
41	70	partial

Table A-6 Velocity and penetration type for 4-gr RCC 1.702-mm fillet radius projectiles

Shot no.	Velocity (m/s)	Penetration
1	123	complete
2	92	complete
3	69	partial
4	76	complete
5	64	complete
6	49	partial
8	81	complete
9	49	partial
10	78	complete
11	54	partial
12	63	complete

Table A-6 Velocity and penetration type for 4-gr RCC 1.702-mm fillet radius projectiles (continued)

Shot no.	Velocity (m/s)	Penetration
14	72	complete
15	58	partial
16	74	complete
17	57	partial
18	66	partial
19	71	complete
20	58	complete
21	58	partial
22	71	complete
23	70	complete
24	50	partial
25	50	partial
26	70	partial
27	56	partial
28	68	complete
29	58	complete
30	70	complete
31	58	partial
32	75	complete
33	50	partial
34	78	complete
35	50	partial
36	73	complete
37	59	partial
38	63	complete
39	58	complete
40	75	complete
41	55	partial

List of Symbols, Abbreviations, and Acronyms

ECH	Enhanced Combat Helmet
IED	improvised explosive device
L	length
LED	light-emitting diode
OD	outer diameter
RCC	right circular cylinder
UHMWPE	ultra-high molecular weight polyethylene
v	velocity

1 (PDF) DEFENSE TECHNICAL INFORMATION CTR DTIC OCA

2 (PDF) CCDC ARL
IMAL HRA
RECORDS MGMT
FCDD RLD CL
TECH LIB

1 (PDF) GOVT PRINTG OFC
A MALHOTRA

34 (PDF) CCDC ARL
FCDD RLW MA
J LASCALA
J SANDS
E WETZEL
L LONG
T BOGETTI
E SANDOZ-ROSADO
K STRAWHECKER
J TZENG
S BOYD
M YEAGER
C F YEN
J CAIN
A QUABIL
J STANISZEWSKI
T PLASITED
D O'BRIEN
B PATTERSON
FCDD RLW MB
J CLINE
GAZONAS
B LOVE
P MOY
T WALTER
FCDD RLW ME
S SILTON
D HARRIS
J SWAB
P PATEL
T TAYLOR
FCDD RLW MG
J LENHART
J YU
FCDD RLW PB
C HOPPEL
T ZHANG
S SATAPATHY
J P MCKEE
T WEERASOORIYA